21

Sintering Process and Its Mechanism of MgB_2 Superconductors

Zongqing Ma and Yongchang Liu
Tianjin Key Lab of Composite and Functional Materials,
School of Materials Science & Engineering,
Tianjin University, Tianjin,
P R China

1. Introduction

1.1 The phase formation mechanism of MgB_2 during sintering

The superconductivity at 39 K discovered in MgB_2 among simple binary chemical composition attracted much interest in its fabrication techniques and practical applications [1]. MgB_2 superconductor exhibits many impressive properties such as highest critical temperature amongst intermetallic superconductors which means low cooling costs, impressive grain boundary transparency to the flow of current which leads to greater critical current density [2-4], comparatively large coherence length which allows a better Josephson junction fabrication, low material cost which will lead to a cheaper superconductor technology, simple crystal structure, etc. Hence, MgB_2 superconductors, especially the MgB_2 wires and coils, have the outstanding potential to be integrated into diverse commercial applications, such as, magnetic resonance imaging (MRI) [5, 6] , fault current limiters (FCL), Josephson junctions and SQUID [7, 8, 9], transformers, motors, generators, adiabatic demagnetization refrigerators, magnetic separators, magnetic levitation applications, energy storage, and high energy physical applications. But the MgB_2 itself is mechanically hard and brittle and therefore not amenable to drawing into the desired wire and tape geometry. Thus, the powder-in-tube (PIT) technique that was used to make the Y-Ba-Cu-O oxide superconductor has been employed in the fabrication of MgB_2 wires and tapes these years [10-14]. So far, in-situ sintering, including the in-situ PIT, from the mixture of magnesium and boron is the major method to fabricate MgB_2 superconductors (bulks, wires and tapes). The corresponding sintering parameters have a significant influence on the superconducting properties of MgB_2. Thus it is necessary to investigate the sintering mechanism of MgB_2 superconductors.

The reaction process and MgB_2 phase formation mechanism during the sintering have been studied by different methods, such as differential thermal analysis (DTA) [15-21], *in-situ* XRD measurement [22-25], *in-situ* resistance measurement [26, 27] and temperature dependent magnetization (M–T) measurements [28].

1.2 Sintering of Mg-B precursor powders over a wide temperature range

It can be seen from the DTA data of the Mg + $2B_{amorphous}$ precursor composition shown in Fig. 1 that the first exothermic peak occurs in the temperature range below 650 ^{o}C (the

melting point of Mg) for samples heated at either 20 °C /min or 5 °C /min [29]. Previous studies have suggested different origins of this peak; some speculate that it is due to the reaction between Mg and impurity B_2O_3 in the original B powder [30, 31], whereas others suggest that it is associated with the solid-solid reaction between Mg and B [16, 18]. In general, there is consensus about the origin of the second and third DTA peaks, which are due to melting of Mg and the liquid-solid reaction between and B, respectively.

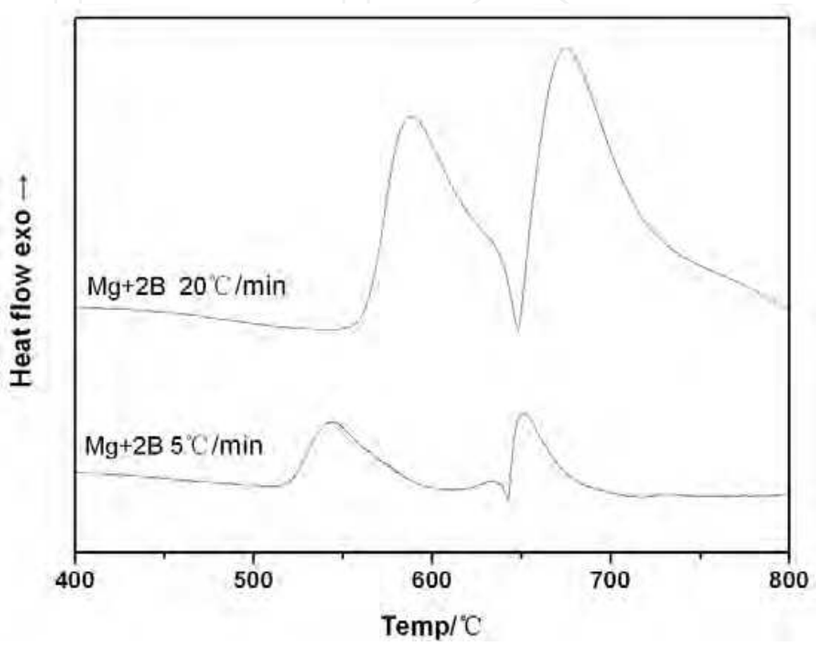

Fig. 1. The measured thermal analysis curves during the sintering of Mg + 2B sample with heating rates of 20 °C·min^{-1} and 5 °C·min^{-1}[29].

With aim of clarifying the origin of first exothermic peak in the DTA curves, the phase evolution of Mg + $2B_{amorphous}$ system was detected by in-situ X-ray diffractometer (XRD) during the sintering up to 750 °C and the measured results are shown in Fig. 2. It is found that obvious MgB_2 phase peaks can be recognized only after 550 °C. In fact, all the measured results of in-situ resistance, *in-situ* XRD and the temperature dependent magnetization during sintering of a mixed powder of Mg : B = 1 : 2 indicate that the MgB_2 phase begins to form before the Mg melting [22, 24, 25, 27, 28]. In this case, the exothermic peak in the DTA curves before the Mg melting occurs, and should be attributed to the solid-solid reaction between Mg and B. The phase formation of MgB_2 during the sintering process, therefore, proceeds via solid-solid reaction, Mg melting and, finally, liquid-solid reaction.

Observing the in-situ XRD patterns in Fig. 2 carefully, a lot of Mg is still present as primary phase in the Mg+2B sample sintered at 600 °C. The result implies that the MgB_2 phase formed at the solid-solid reaction stage is limited due to the low atomic diffusion rate in the solid state. On the other hand, also as shown in Fig. 2, MgB_2 phase forms on a much larger scale and becomes primary phase immediately following completion of the melting of Mg when the sintering temperature reaches 650 °C. As a result, in order to obtain complete MgB_2 phase rapidly, the MgB_2 superconductors were generally synthesized by sintering at high temperature in the past decade.

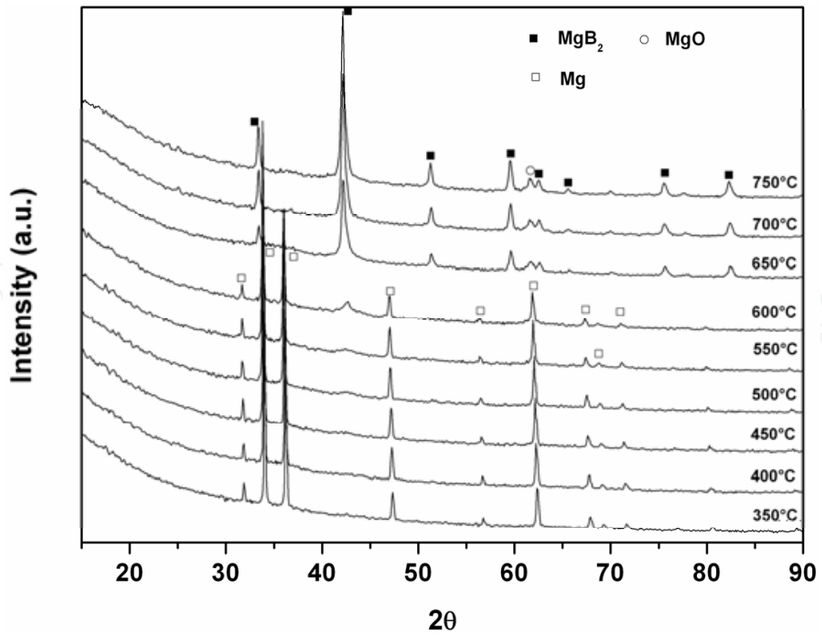

Fig. 2. The in-situ XRD patterns of (a) Cu-doped MgB_2 sample and (b) undoped MgB_2 sample.

1.3 Sintering process and mechanism of MgB_2 superconductors at high temperature

Since most of MgB_2 superconductors are prepared by sintering at high temperature, it makes sense to investigate their phase formation process and sintering mechanism at high sintering temperature. At high temperature, the liquid-solid reaction between Mg and B is activated following completion of the melting of Mg. The MgB_2 phase formation mechanism at this stage should be very different to that at the solid-solid reaction stage due to the presence of the Mg melt.

A large number of small MgB_2 grains exist in the bulk material after the solid-solid reaction, together with residual Mg and B particles. When the sintering temperature is above 650 ^{o}C, residual Mg melted and the flowing liquid phase (Mg) increased the diffusion rate of atom and enlarged the contact area of reactants, which leads to a strong and complete reaction between residual Mg and B.

According to our previous study [17], this solid-liquid reaction stage follows Ostwald ripening mechanism and includes three important processes [32]:

i. *rearrangement of particles*. The molten Mg helps individual particles to slip, spin and reassemble;
ii. *solid-liquid reaction*. The residual B particles are entrapped by the molten Mg, which promotes a strong instantaneous contact reaction;
iii. *solution-reprecipitation and grain growth*. Small MgB_2 grains generally have a higher solubility in the liquid phase than larger grains [33] and will dissolve first in the Mg melt to yield an over-saturated solution. This will lead to the precipitation of MgB_2 on the surface of existing MgB_2 grains, which will lead to further grain growth, as shown in Fig. 3.

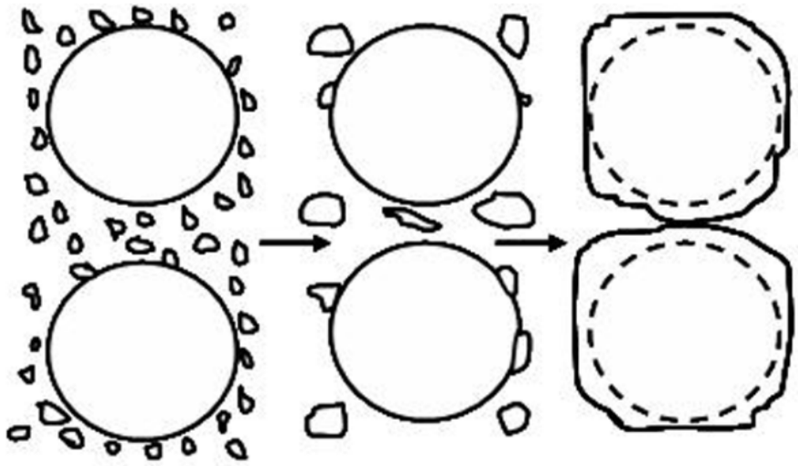

Fig. 3. Schematic illustration of the solution-reprecipitiation and growth process of grains during the liquid-solid stage [17].

According to above discussion, when the sintering temperature rise to 750 °C, the ending point of solid-liquid reaction in the DTA curve (see Fig. 1), complete MgB_2 phase can be obtained (see Fig. 2) and most of MgB_2 grains tend to be regular hexagon in the sample (see Fig. 4, the SEM image of sample sintered at 750 °C).

It is very difficult to calculate the kinetic parameters exactly from the DTA analysis data due to the overlap between the Mg melting and liquid-solid reaction thermal peaks. Hence, only limited kinetic information calculated from the *in-situ* X-ray diffraction measurement has been reported for the liquid-solid reaction between Mg and B. DeFouw *et al.* Ref. [23] reports that the liquid-solid reaction between Mg and B under isothermal conditions can be described by diffusion-controlled models of a reacting sphere with kinetics characterized by diffusion coefficients that increase with temperature from 2×10^{17} to 3×10^{16} s^{-1}, with associated activation energies of 123 ~ 143 $kJ \cdot mol^{-1}$. However, a very high heating rate was used in these studies to prevent the reaction between Mg and B occurring below a certain temperature (above the melting point of Mg). As a result, the sintering environment might be quite different from that in traditional sintering methods.

Previous studies on the phase formation mechanism of MgB_2 during liquid-solid sintering between Mg and B are deficient, and further investigation is necessary in addition to advanced test methods.

1.4 Conventional solid-state sintering of MgB_2 superconductors at low temperature

Though high-temperature sintering is the most popular method of synthesizing MgB_2 superconductors till now, the high volatility and tendency of Mg to oxidize at high temperature pose significant challenges to the fabrication of MgB_2 superconductors that exhibit excellent superconductive properties since these processes tend to generate voids and MgO impurities during in-situ sintering. Thus, recent studies have addressed the low-temperature preparation of MgB_2 superconductors in an attempt to reduce the oxidation and volatility of Mg.

As discussed above, the formation of the MgB_2 phase begins at a temperature below the melting point of Mg, which offers the prospect of sintering MgB_2 superconductors at relatively low temperature (i.e. below the melting point of Mg) in an attempt to avoid problems associated with the strong volatility and oxidation of Mg at high temperature. Rogado *et al.* [34] initially fabricated superconducting bulk MgB_2 samples by conventional solid state sintering at a temperature as low as 550 °C (see Fig. 5). This process required a sintering time of 16 hours to form the complete bulk MgB_2 phase, and the samples exhibited inferior superconducting properties than those sintered at high temperature. However, the result indicates that it is possible to fabricate MgB_2 superconductors at low temperature and this work resulted in increased attempts world-wide to develop a low-temperature sintering process for both undoped and doped MgB_2 bulk superconductors.

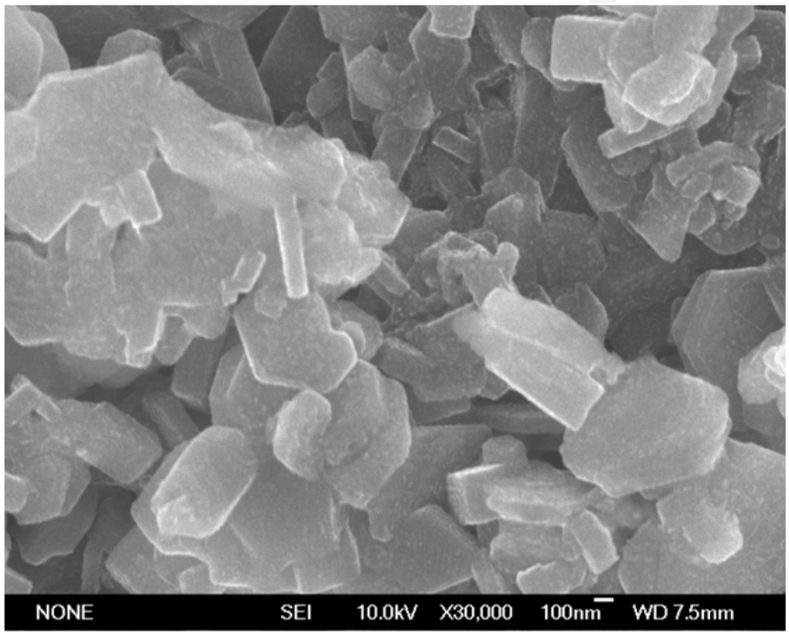

Fig. 4. SEM image of MgB_2 sample sintered at 750 °C.

Yamamoto *et al.* [35] found that MgB_2 bulk superconductors prepared by solid state sintering at 600°C for 240 h exhibited improved critical current densities at 20 K (see Fig. 11). This study confirmed the potential of the low temperature sintering technique for the fabrication of bulk MgB_2 superconductors. It also established that poor crystallinity is found to enhance H_{c2}, H_{irr} and J_c in MgB_2 at high fields, whereas strong grain connectivity, reduced MgO impurity content and a smaller grain size increases J_c at low fields.

MgB_2 wires and tapes with improved H_{irr} and J_c can also be prepared by low temperature sintering by an *in-situ* PIT technique. Goldacker *et al.* [36] reports the synthesis of thin, steel-reinforced MgB_2 wires with very high transport current densities at only 640 °C. These authors suggest that the low-temperature annealing could lead to a fine grain structure and a superconducting percolation path with very high associated critical current density. Moreover, the observation of a dramatically-reduced reaction layer between the filament and sheath in their samples is very promising for the production of filaments with small diameters in mono- and multifilamentary wire.

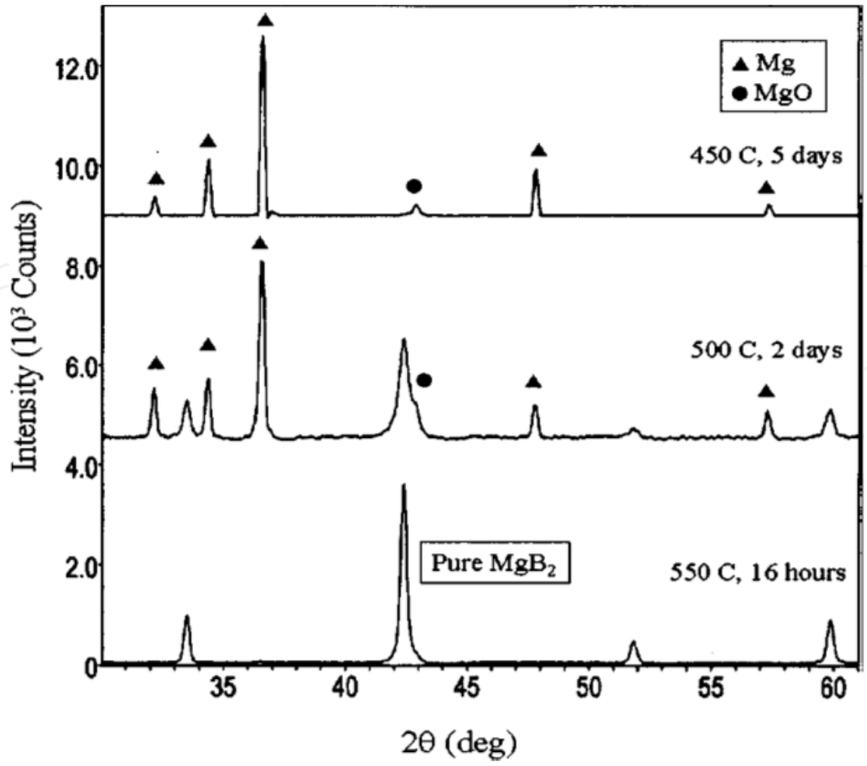

Fig. 5. Powder x-ray diffraction patterns of MgB_2 samples prepared using different heating conditions. Markers are placed above the peaks corresponding to Mg and MgO impurities. The unmarked peaks correspond to MgB_2 (from Ref. [34]).

Recently, a new process, called two-step heat-treatment, has been developed to fabricate undoped MgB_2 bulk superconductors [37]. In this process, short high-temperature sintering at 1100 °C is followed by low-temperature annealing. Samples prepared by this method exhibit, uniquely, well-connected small grains with a high level of disorder in the MgB_2 phase, which yields an in-field J_c of nearly one order of magnitude higher than for the samples prepared by single-step sintering at high or low temperature. However, the applicability of the two-step heat-treatment to the fabrication of MgB_2 wires has yet to be investigated.

To summarize, these MgB_2 superconductors synthesized at low temperature were generally cleaner and denser than the same samples sintered at high temperature due to the reduced volatility and oxidation of Mg, which could improve the connectivity between MgB_2 grains. Moreover, sintering at low temperature can also obtain the refined MgB_2 grains, which obviously strengthens the grain-boundary pinning. Both of factors are bound to result in the improvement of critical current density in the low-temperature sintered samples compared to the typical high-temperature sintered samples. From this point of view, the low-temperature synthesis might be the most promise and effective method in obtaining the higher J_c in MgB_2 superconductors. Hence, it makes sense to clarify the phase formation mechanism of MgB_2 during the low-temperature sintering.

1.5 Sintering kinetics of MgB_2 superconductors at low temperature

Analysis of the kinetics of the sintering process can be performed based on the DTA data using different computational methods. Yan *et al.* [18] calculated the activation energy of the solid-solid reaction at low sintering temperature using the Ozawa–Flynn–Wall and Kissinger as 58.2 and 72.8 kJ·mol^{-1}, respectively. The value of the pre-exponential factor calculated using the Kissinger method is 2.0×10^{15} s^{-1}. They also report that the activation energy increases parabolic as the reaction progresses [18]. However, the study by Shi *et al.* [19] draws different conclusions to those of Yan et al. These authors use a new kinetic analysis (based on a variant on the Flynn-Wall-Ozawa method) under non-isothermal conditions and suggest that the solid-solid reaction between Mg and B powders follows an instantaneous nuclei growth (Avrami–Erofeev equation, n = 2) mechanism. The values of E decrease from 175.4 to 160.4 kJ·mol^{-1} with the increase of the conversion degrees (α) from 0.1 to 0.8 in this model. However, the activation energy (E) increases to 222.7 kJ·mol^{-1} [19] again as the conversion degree reaches 0.9.

On the other hand, the solid-solid reaction between Mg and B exothermal peak is partly overlapped with the Mg melting endothermic peak in the DTA curves. This phenomenon makes it difficult to calculate the kinetics parameters exactly from the thermal analysis data and also could be the reason why the previous results are different from different research groups. It is necessary to further investigate the phase formation mechanism of MgB_2 during the low-temperature sintering combined with advanced test methods.

In our recent work [38], in-situ X-ray diffraction technique is used to measure the degree of reaction between Mg and B as a function of time at several certain temperatures below Mg melting, respectively. Based on these isothermal data, the kinetics analysis of MgB_2 phase formation during the low-temperature sintering is carried out.

Bulk samples of MgB_2 were prepared by a solid-state sintering method using amorphous boron powder (99% purity, 25μm in size), magnesium powder (99.5% purity, 100 μm in size). Several reaction temperatures in the range of 550~600 ^{o}C, below the melting point of Mg, were chosen as the isothermal holding temperatures. Then the samples were fast-heated to the chosen temperature with a rate of 50 ^{o}C/min in order to prevent significant reaction between Mg and B before arriving at the isothermal annealing temperature. The x-ray diffraction measurement started as soon as the sample temperature reached the certain isothermal temperature and it will detect the sample every 15 min till the reaction is over. The weight fraction of synthesized MgB_2 which corresponds to the degree of reaction was calculated from the XRD data of sample obtained after different soaking time according to the External Standard Method.

Fig. 6 illustrates the typical X-ray diffraction patterns of the Mg-B sample isothermally annealed at 575 ^{o}C for different periods. One can see that no organized MgB_2 peak can be observed when the temperature just reaches 575 ^{o}C. It implies that the reaction between Mg and B did not occur during the rapid heating to the final isothermal holding temperature. As the holding time prolonging, the MgB_2 phase appears and increases gradually while the Mg phase decreases. However, the increase in the intensity of MgB_2 peaks becomes very slow and even stops when it reaches a certain degree despite of longer holding time (ie. longer than 480 min). Similar behavior is also found in the isothermal annealing experiments at 550 ^{o}C and 600 ^{o}C (the XRD patterns in not shown here).

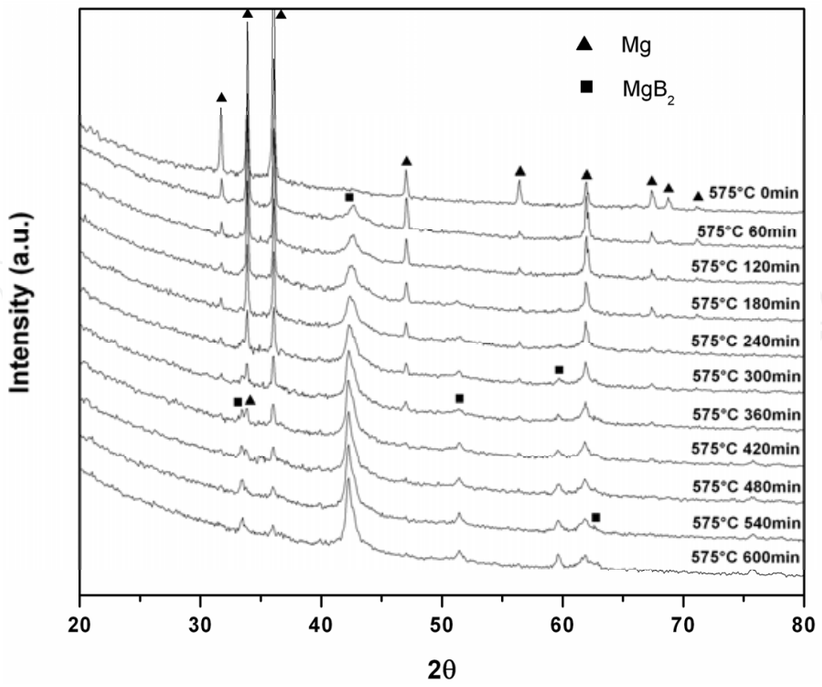

Fig. 6. Typical X-ray diffraction patterns of the Mg-B powder specimen isothermally annealed at 575 °C for different periods [38].

According to the XRD data, the weight fraction of the synthesized MgB_2 phase, which is considered as the degree of reaction, is calculated using the External Standard Method. Plots of degree of reaction vs. time are given in Fig. 7 for isothermal sintering at 550 °C, 575 °C

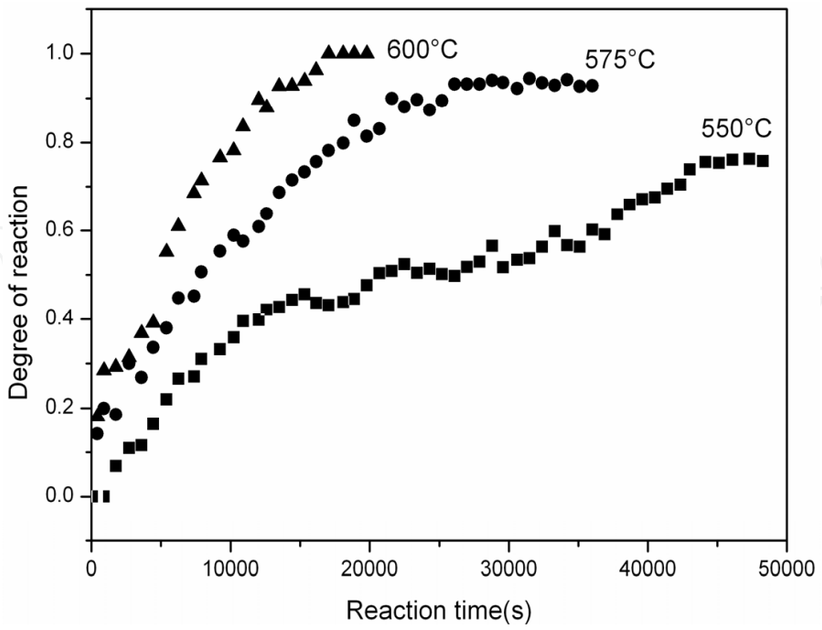

Fig. 7. Plots of degree of reaction vs. time isothermally-annealed Mg-B powder specimens at 550 °C, 575 °C and 600 °C, respectively [38].

and 600 °C, respectively. At 550 °C and 575 °C, the reaction seems stop even though the degree of reaction is still below 100% and there is residual Mg and B in the sample (see Fig. 6). It means that at the final stage of isothermal heating in present work, the reaction rate is so slow that it is difficult to observe the increase in the degree of reaction. At each isothermal annealing temperature, it can be also found that the reaction rate becomes slower and slower with the reaction time increasing and the degree of reaction seems unchanged at last.

Based on these isothermal data, kinetics analysis of the MgB_2 phase formation during the low-temperature sintering is carried out. Early kinetics studies employed the currently-accepted kinetic equation:

$$\frac{d\alpha}{dt} = k(T) f(\alpha) \tag{1}$$

Where t represents time, a is the degree of reaction, T is the temperature, k(T) is the temperature-dependent rate constant and $f(a)$ is a function that represents the reaction model. $k(T)$ can be described as:

$$k(T) = A \exp(-\frac{E}{RT}) \tag{2}$$

Where A is the pre-exponential factor, E is the activation energy and R is the gas constant.

Integrating Eq. (1), it comes:

$$g(\alpha) \equiv \int_0^{\alpha} [f(\alpha)]^{-1} d\alpha = k(T)t \tag{3}$$

Where $g(a)$ is the integral form of $f(a)$.

After substitution for $k(T)$ and rearranging, it yields:

$$\ln(t) = \frac{E}{RT} + \ln\left[\frac{g(\alpha)}{A}\right] \tag{4}$$

It needs different reaction time to reach certain degree of reaction at different isothermal holding temperatures. According to Eq. (4), at certain degree of reaction, one can plot the $lnt \sim 1/T$ and then do a linear fit. Following this way, the activation energy (E) can be obtained without referring to the reaction modes. Table 1 illustrates the reaction time and activation energy at different degree of reaction of the Mg-B sample. It is recognized that the activation energy (E) firstly decreases when a changes from 0.20 to 0.40 and then increases again when a changes from 0.50 to 0.80. It is indicated that the reaction between Mg and B at low temperature is not controlled by only one kinetics reaction model. At different stage of reaction, the kinetics model is varied.

In order to determine the kinetic modes of the reaction between Mg and B during the low-temperature sintering, Model fitting method is performed. Following this method, The determination of the $g(a)$ term is achieved by fitting various reaction models to experimental data. As described below in Eq. (5), the relationship between $g(a)$ and t should be linear.

$$g(\alpha) = A\exp(-\frac{E}{RT})t \tag{5}$$

Set of alternate reaction models is linearly-fitted to the experimental data obtained from the is-situ X-ray diffraction results at 575 °C and then obtained results are collected in Table 2. The coefficient *r* of the contracting cylinder, contracting sphere and one-dimensional diffusion models are the better ones. According the Eq. (5), the intercept *t* during the linear fitting should be zero. But the intercept of contracting cylinder model is 0.0821, which is too high compared to 0. And the corresponding value of *r* is also not as good as the case in the Contracting sphere model. Hence, the contracting cylinder model is ignored here. On the other hand, the coefficient *r* of the contracting sphere is better than that of the one-dimensional diffusion model. But the intercept of one-dimensional diffusion model is more near to 0 than that of the contracting sphere model.

Degree of reaction (*a*)	Reaction time (*t*) at 550 °C (s)	Reaction time (*t*) at 575 °C (s)	Reaction time (*t*) at 600 °C (s)	Activation energy (*E*) (kJ/mol)
0.20	5200	1500	520	275.39
0.30	6700	3600	2250	130.58
0.40	11700	5700	4500	114.75
0.50	21000	8100	5100	169.71
0.60	36000	11700	6150	181.71
0.70	42300	14100	7800	202.63
0.80	46800	18900	10260	211.74

Table 1. The reaction time (*t*) and activation energy (*E*) at different degree of reaction (α) during the low-temperature sintering of the Mg-B powders [38].

Reaction model	*G(a)*	Slope (*b*)	*r*-square	Intercept (*a*)
One-dimensional diffusion	α^2	3.49×10^{-5}	0.9851	-0.0165
Two-dimensional diffusion	$[1-(1-\alpha)^{1/2}]^{1/2}$	2.14×10^{-5}	0.9568	0.3411
Mampel (first order)	$-\ln(1-\alpha)$	9.20×10^{-5}	0.9720	-0.0060
Avrami-Erofeev	$[-\ln(1-\alpha)]^{1/2}$	4.53×10^{-5}	0.9830	0.4432
Avrami-Erofeev	$[-\ln(1-\alpha)]^{1/3}$	3.06×10^{-5}	0.9730	0.6088
Avrami-Erofeev	$[-\ln(1-\alpha)]^{1/4}$	2.32×10^{-5}	0.9648	0.6977
Contracting cylinder	$1-(1-\alpha)^{1/2}$	2.54×10^{-5}	0.9855	0.0821
Contracting sphere	$1-(1-\alpha)^{1/3}$	2.05×10^{-5}	0.9869	0.0417
Power law	$\alpha^{3/2}$	3.39×10^{-5}	0.9779	0.0711
Power law	$\alpha^{1/2}$	2.09×10^{-5}	0.9042	0.4934
Power law	$\alpha^{1/3}$	1.57×10^{-5}	0.8821	0.6276
Power law	$\alpha^{1/4}$	1.25×10^{-5}	0.8699	0.7061

Table 2. Linear fitting results of the experimental data obtained from the in-situ X-ray diffraction results at 575 °C by adopting alternate reaction models [38].

According to Eq. (4), the intercept of plot *lnt ~1/T* ($\ln(\frac{g(\alpha)}{A})$), can be obtained from the linear fitting. At certain degree of reaction, if the *g(a)* is given, the value of *A* can be calculated. Then $k(T) = A\exp(-\frac{E}{RT})$ can also be determined at certain temperatures. The calculated value of *k*(*T*) should be consistent with the linear fitted slope of plot *g*(*a*)~*t* if the given *g*(*a*) is the valid reaction model.

Following this method, we verify these two models discussed above at 575°C. At the initial stage (*a*=0.20) of reaction, for contracting sphere model ($1-(1-\alpha)^{1/3}$), the calculated *k*(*T*) is 2.09×10^{-5}, which is comparable to the corresponding value of slope given in Table 2. In the case of one-dimensional diffusion model (α^2), the calculated *k*(*T*) is 1.19×10^{-5}, which is much smaller than the corresponding value of the slope presented in Table 2. At the middle stage ((*a*=0.50) of reaction, the calculated value of *k*(*T*) from the contracting cylinder model is 2.18×10^{-5}, which is still comparable to the corresponding value of slope. For the one-dimensional diffusion model, the calculated *k*(*T*) is 2.64×10^{-5}, which is smaller than the corresponding value given in Table 2. However, at the final stage (*a*=0.80), the calculated *k*(*T*) from the one-dimensional diffusion model is 3.62×10^{-5}, which is more consistent with the corresponding value presented in Table 2 than that in the case of the contracting cylinder model (the calculated value is 2.33×10^{-5}).

Hence, one can say that the reaction between Mg and B during low-temperature sintering is firstly mainly controlled by the contacting sphere model, which is a kind of the phase boundary reaction mechanism. As the reaction prolongs, the one-dimensional diffusion model, one kind of diffusion-limited mechanism, gradually becomes dominant.

In our previous study [39], we have investigated the MgB_2 phase formation process during the sintering based on the phase identification and microstructure observation. It is found that the sintering 'necks' between individual Mg and B particles occurs at the first stage of the sintering. Then the solution active regions form at the sintering necks. With the isothermal heating prolonging, a few Mg and B atoms in the solution active regions can be activated and react with each other. The activated atoms are limited at this initial stage and thus the reaction rate is slow and mainly determined by the phase boundary reaction mechanism. Meanwhile, an MgB_2 phase layer is gradually formed at the sintering necks between Mg and B particles and the Mg atoms have to diffuse through the whole MgB_2 phase layer to reach the reaction interface, , as shown in Fig. 8. As the reaction prolonging, the synthesized MgB_2 layer becomes thicker and thicker, and it should be more and more difficult for Mg atoms to reach the reaction interface through diffusion. Finally, the reaction rate is controlled by the diffusion-limited mechanism. As a result, the reaction rate becomes slower and slower and it takes a very long time to be totally completed due to the slow diffusion rate of Mg. The corresponding activation energy is also decreased firstly and then increased again during the whole reaction process, as discussed above. It is also the reason why the residual Mg is still present even after holding for 10 h at 575 °C.

Based on above analysis and compared with previous studies [18, 19] in which they propose the reaction is controlled by single mechanism, the varied mechanisms are more valid and more consistent with the actual sintering process. The value of activation energy in present

work is also comparable to the calculated value in Shi et al.'s study [19] whereas the models are different from theirs. But in their study, the activation energy is calculated using a model-free method, just as in our work.

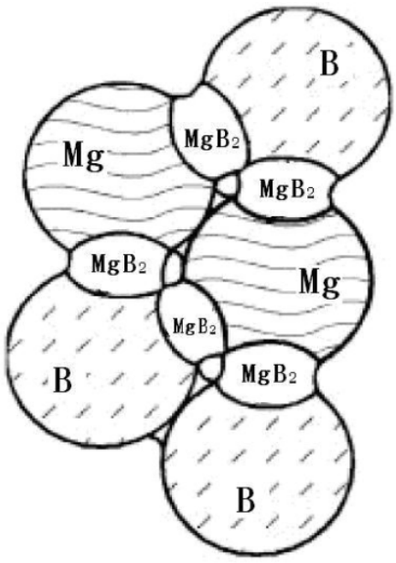

Fig. 8. Schematic illustration of solid-solid reaction between Mg and B particles based on the inter-diffusion mechanism [39].

Based on above discussion, it is concluded that the reaction between Mg and B during the low-temperature sintering is controlled by varied mechanisms. At initial stage, the reaction rate is mainly determined by the phase boundary reaction mechanism. As the reaction prolonging and the synthesized MgB_2 layer increasing, the diffusion-limited mechanism gradually becomes dominant. The corresponding activation energy is also decreased firstly and then increased again.

2. Accelerated sintering of MgB_2 with different metal and alloy additions at low temperature

According to the above sintering mechanism, the reaction between magnesium and boron at low temperature took a very long time to form the complete MgB_2 phase as the result of the low diffusion rate of Mg atom at solid state. In order to rapidly synthesize the complete MgB_2 phase through the low-temperature sintering, improving the diffusion efficiency of Mg atoms to the reaction interface is the key point, especially at the final stage of the sintering.

2.1 The influence of different metals and alloys on the sintering process and superconductive properties of MgB_2

In order to accelerate the diffusion rate of Mg atoms and thus improve sintering efficiency of MgB_2 at low temperature, different metals and alloys dopants were added into Mg-2B sintering system by world-wide research groups.

Shimoyama *et al.* [40] found that a small amount of silver addition decreases dramatically the reaction temperature of magnesium and boron in the formation of bulk MgB_2 without degradation of either the critical temperature or the critical current density. Although the added silver forms an Ag-Mg alloy after the heat treatment, these impurity particles exist mainly at the edge of voids in the sample microstructure and therefore do not provide a significant additional restriction to the effective current path. Accordingly MgB_2 bulks with excellent J_c properties have been fabricated at a temperature as low as 550 °C with the 3 at.% Ag doping. The sintering time of doped samples is also reduced significantly compared to that required for undoped samples fabricated by low temperature sintering. This effectively widens the processing window for the development of practical, low-cost MgB_2 superconductors by reaction at low temperature [40].

Hishinuma *et al.* [41] synthesized Mg_2Cu-doped MgB_2 wires with improved J_c by sintering at low temperature for 10 h. They found that the formation of the MgB_2 phase is improved due directly to the lower melting point of Mg_2Cu (568 °C) than Mg (650 °C), which can promote the diffusion of Mg in the partial liquid (the MgB_2 phase forms by the diffusion reaction between released Mg from Mg_2Cu and amorphous B powder [41]). The J_c of sample prepared in this way can be improved further in Mg_2Cu-doped MgB_2 wires by sintering at lower temperature (450 °C) for longer time (more than 100 h). The maximum core J_c value of these samples was found to be over 100, 000 A cm^{-2} at 4.2 K in a magnetic field of 5 T for a tape sintered for 200 h. Bulk MgB_2 has been fabricated successfully in other studies by Cu-doping and sintering at 575 ^oC for only 5 h [42]. Thermal analysis indicates that the Mg-Cu liquid forms through the eutectic reaction between Mg and Cu at about 485 °C, which leads to the accelerated formation of MgB_2 phase at low temperature. The SEM images of the sintered Cu-doped samples are shown in Fig. 9. It is observed that the undoped sample is porous and consists of small irregular MgB_2 particles and large regular Mg particles which are in poor connection with each other (see Fig. 9a). On the other hand, the MgB_2 particles of the doped sample become larger and more regular accompanying with the increasing amount of Cu addition. The doped samples also become denser with the amount of Cu addition increasing for the reason that the MgB_2 particles are in better connection with each other and give birth to less voids (see Figs. 9b-9d). Especially, as shown in the Fig. 9d, the MgB_2 grains in the $(Mg_{1.1}B_2)_{0.9}Cu_{0.1}$ sample exhibit platy structure with a typical hexagonal shape [42]. The high J_c in MgB_2 samples doped with Cu is attributed mainly to the grain boundary pinning mechanism that results from the formation of small MgB_2 grains during low temperature sintering. As with the Ag-doped samples, the concentration of Mg-Cu alloy in these samples tends to form at the edge of voids in the microstructure and does not degrade significantly the connectivity between MgB_2 grains, which contributes directly to enhanced J_c. Recently, the addition of Sn to the precursor powder has also been observed to assist the formation of the MgB_2 phase during low temperature sintering, and bulk Sn-doped MgB_2 prepared at 600 ^oC for 5 h exhibit good values of J_c [43].

Interestingly, although Ag and Sn addition can form a local eutectic liquid with the Mg precursor at lower temperature than the addition of Cu, the Cu has been found to play a more effective role in the improvement of MgB_2 phase formation than Ag and Sn at low temperature. The Cu-doped samples take significantly less time to form the primary MgB_2 phase than those containing similar concentrations of Ag or Sn at a similar sintering

temperature [40, 42, 43]. Grivel *et al.* [44] observed a similar phenomenon in a study of the effects of both Cu and Ag on the kinetics of MgB_2 phase formation. The addition of 3 at.% Cu or Ag to a precursor mixture consisting of Mg and B powders results in a significant increase of MgB_2 phase formation kinetics in the temperature range below the melting point of Mg. The MgB_2 phase forms more rapidly in the precursors containing Cu than those containing Ag. These authors suggest that this behavior might be related to the lower solubility limit of Cu in solid Mg, compared to the case of the Mg-Ag system [44].

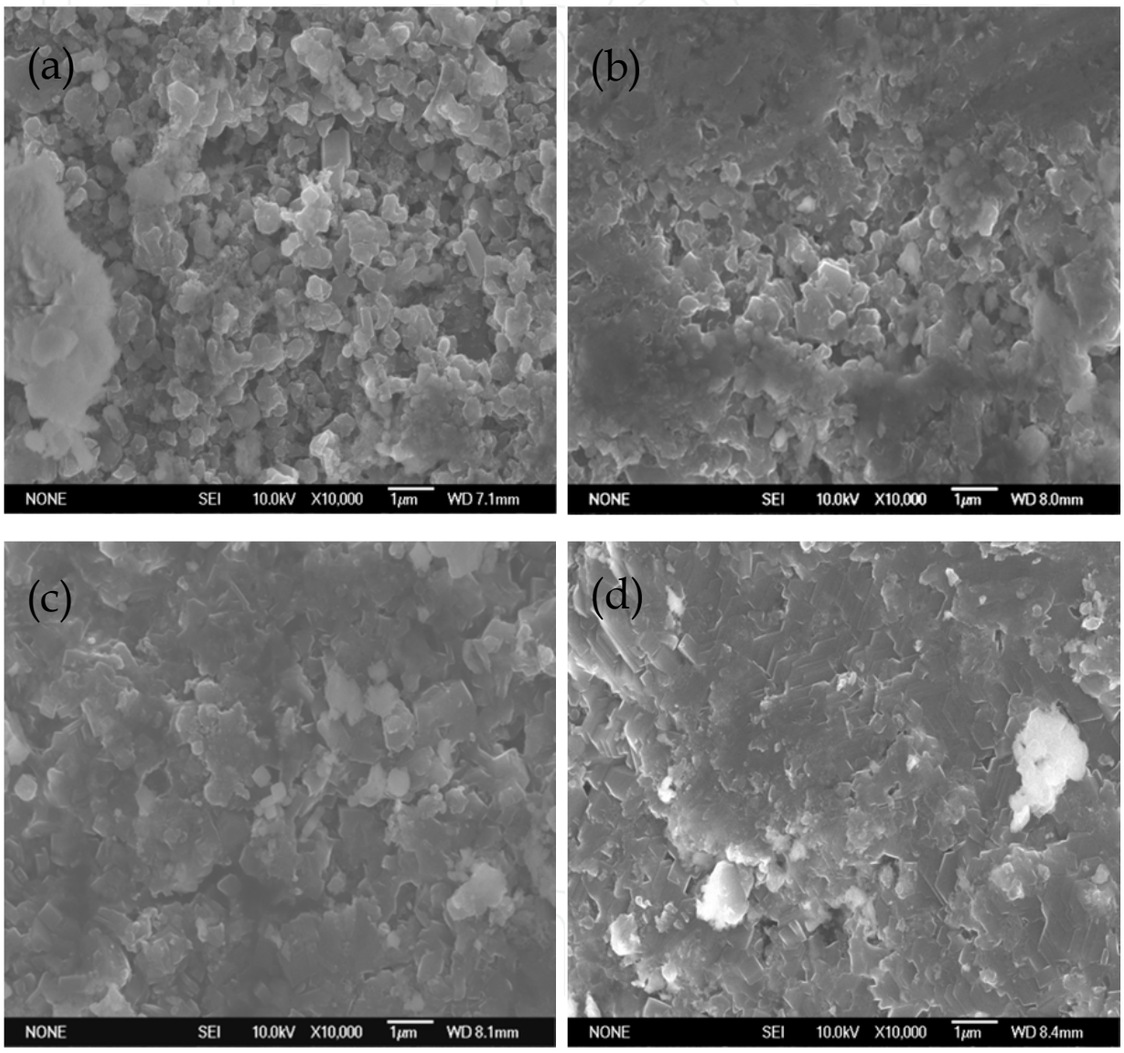

Fig. 9. SEM images of the microstructures of the $(Mg_{1.1}B_2)_{1-x}Cu_x$ samples sintered at 575 °C for 5 h with (a) x = 0.0, (b) x = 0.03, (c) x = 0.05 and (d) x = 0.10, respectively [42].

Based on the above discussion, the assisted sintering of MgB_2 with different metal or metal alloy additions at low temperature is convenient from a practical processing point of view and also reduces the processing time. In addition, these additives tend to be cheap and yield MgB_2 samples with improved J_c. Therefore, this technique appears to be the most promising way of preparing practical, low-cost MgB_2 superconductors at low temperature, compared to the use of different Mg-based precursors and the ball milling pretreatment of precursor powders.

2.2 The mechanism of metal-accelerated sintering at low temperature

The addition of minor metals or metal alloys additions represents the most convenient, effective and inexpensive way of preparing MgB_2 with excellent superconducting properties at low sintering temperatures. As a result, the accelerated sintering mechanism apparent in the effective processing of these samples should be clarified. The accelerated sintering mechanism of precursors containing Cu, for example, has been studied in detail using thermal analysis and activated sintering theory [44, 45, 46].

As discussed in section 1.1, thermal analysis of the sintering process of undoped MgB_2 reveals three peaks corresponding to solid-solid reaction, Mg melting and solid-liquid reaction (see Fig. 10). A similar process was observed in samples of composition $(Mg_{1.1}B_2)_{1-x}Cu_x$ with x = 0.01, 0.03, 0.05 and 0.10, except that the on-set temperature of each the three peaks decreased gradually with increasing amount of Cu addition. It should be noted that an apparent endothermic peak appears at about 485 ^oC, which is just below the first exothermic peak in the thermal analysis curves of the $(Mg_{1.1}B_2)_{0.90}Cu_{0.10}$ samples. By reference to the binary Mg-Cu phase diagram (see Fig. 11), it is apparent that the Mg-Cu liquid initially forms locally through the eutectic reaction during the sintering process of Mg-Cu-B system, resulting in the appearance of this apparent endothermic peak. The local formation of Mg-Cu liquid in the $(Mg_{1.1}B_2)_{1-x}Cu_x$ samples with x = 0.01, 0.03 and 0.05 is limited for the small amount of Cu added to the precursor, which results in an endothermic signal that is too small to be detected by the thermal analysis measurement in this temperature range [46].

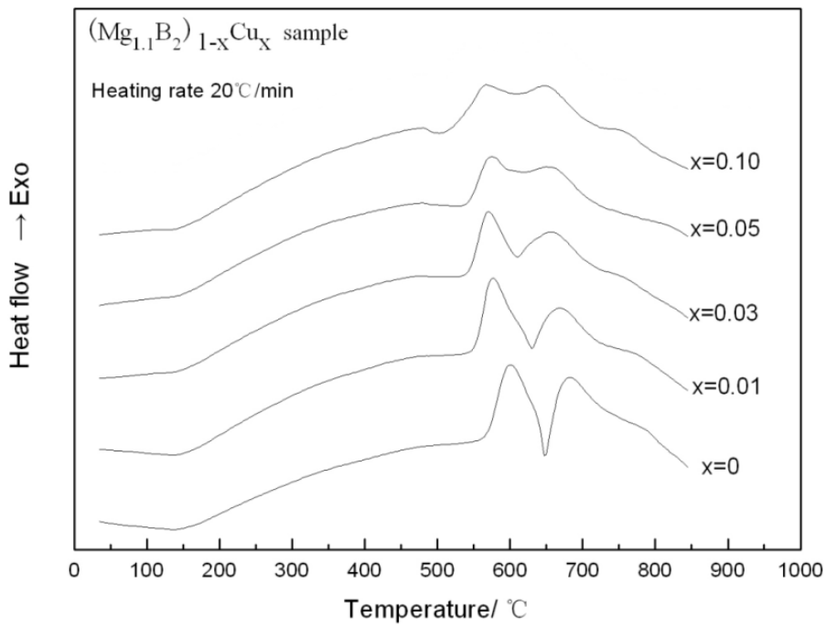

Fig. 10. Measured thermal analysis curves during the sintering of $(Mg_{1.1}B_2)_{1-x}Cu_x$ (with x = 0, 0.01, 0.03, 0.05 and 0.10) samples with an applied heating rate of 20 ^oC /min [46].

This raises the question of how the presence of a local Mg-Cu liquid accelerates the subsequent formation of MgB_2 phase. (in previous studies [45, 46], the accelerated sintering mechanism of MgB_2 with Cu addition is attributed to the activated sintering).

It is known that activated sintering of MgB_2 by chemical doping facilitates either a lower sintering temperature or a shorter sintering time. German *et al.* [45] have proposed the three criteria for activated sintering systems of solubility, segregation and diffusion as follows:

i. *Solubility* The additive A must have a high solubility for the base B, while the base B must have a low solubility for the additive A so that the additive can wet the base particles and then exhibit a favorable effect on diffusion.
ii. *Segregation* During the sintering, the additive must remain segregated at the inter-particle interfaces to remain effective during the entire sintering process.
iii. *Diffusion* The diffusivity of the base metal B in the additive layer must be higher than the self-diffusivity of the base metal B.

Accordingly, an ideal phase diagram for the activated sintering system can be constructed (see Fig. 12). The formation of the MgB_2 phase in the Mg-Cu-B system, is controlled mainly by the diffusion rate of Mg atoms. Only the effect of Cu addition on this diffusion rate is considered to be significant, and the effect of Cu addition on the B atoms can be neglected. Hence, the Mg-Cu-B system can be simplified as an Mg-Cu system for the analysis of the influence of Cu addition on the sintering process. As shown in the Mg-Cu phase diagram (see Fig. 11), Cu addition dramatically decreases the liquidus and the solidus, which implies that the local Mg-Cu liquid can segregate to the interface of Mg particles and therefore meets the *Segregation* criterion in German's study [45]. The high solubility of Cu for Mg (see Figs 11 and 12) enables the Mg-Cu liquid to wet the Mg particles and support the diffusion transport mechanism. As a result, this meets the *solubility* criterion. Generally, the atomic diffusivity in the liquid state is larger than that in the solid state, so the Mg-Cu liquid also meets the *Diffusion* criterion. Collectively, these observations suggest theoretically that the local Mg-Cu liquid meets all the criteria for the diffusion of Mg to B. Cu, therefore, can serve as the activated sintering addition and accelerate the formation of the MgB_2 phase. The conclusion can also be verified by the microstructure observation of the Cu-doped sample sintered at low temperature, as shown in Fig. 13 [46]. It was clear that Cu was concentrated at local region by the edge of voids while Mg was preferentially distributed inside of particles far away from the voids. The result indicated that the Mg-Cu alloys corresponding to the local Cu-Mg liquid during the sintering process mainly concentrated at the edge of voids. Since the void results from the diffusion of Mg atom into B during sintering as mentioned previously [21], the concentration of Mg-Cu alloys at the edge of the voids implied that the Mg-Cu liquid generated and segregated to the interface between Mg particles and B particles at the initial stage of the sintering process and then provided a high transport for the diffusion of Mg into B. After a period of sintering time, Mg was run out and voids formed at the former place of the Mg.

Other metals or metal alloys must first form local liquids with Mg before the formation of MgB_2 phase if they are to serve as activate additives during low temperature sintering. Whether or not these local liquids promote the formation of the MgB_2 phase and activate the sintering mechanism, should be verified by considering the criteria described above (for the case of Cu addition), the ideal phase diagram for the activated sintering system and the binary phase diagram of the added element and Mg. In the section 2.1, the addition of Cu was demonstrated to be more effective than Sn or Ag in accelerating the formation of the

MgB_2 phase at low temperature, even though the latter can form liquid at much lower temperature. Inspection of the relevant binary phase diagram of Sn and Ag with Mg (not shown here) indicates that the solubility limit of Mg in Sn is much lower than that in Cu. Hence, it is more difficult for the Sn-based local liquid to wet the Mg particles and promote the diffusion of Mg according to the *Solubility* criterion. As a result, the activated sintering of MgB_2 with Sn addition is much less efficient than Cu addition. On the other hand, the solubility limit of Mg in Ag is higher than that in Cu and the Ag-based local liquid should wet the Mg particles more easily and accelerate the diffusion of Mg more effectively. However, the solubility limit of Ag in solid Mg is also much higher than for the case of Cu, which means that the amount of local Ag-based liquid present will decrease due to the solution of Ag in the Mg solid. The effect of this is to lower the activated sintering efficiency compared to that obtained for a similar concentration of Cu addition.

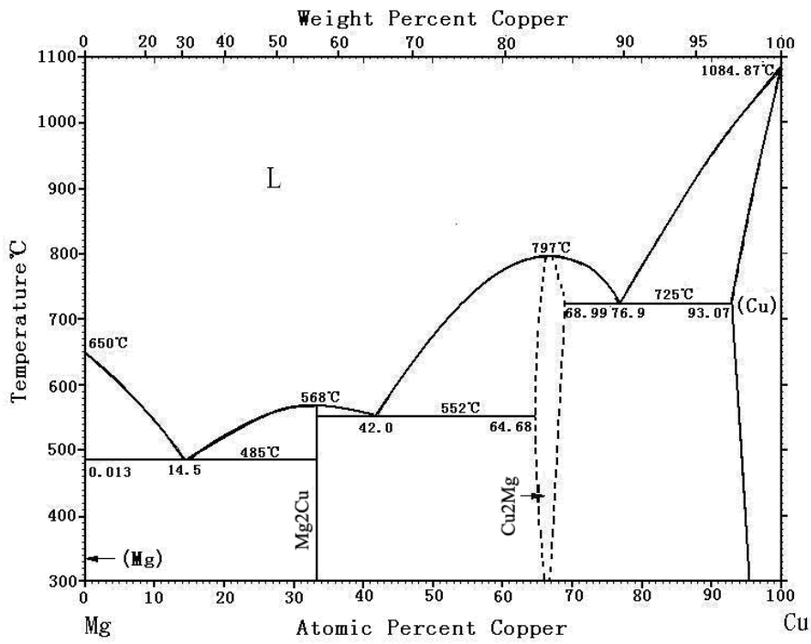

Fig. 11. Binary Mg-Cu phase diagram [48].

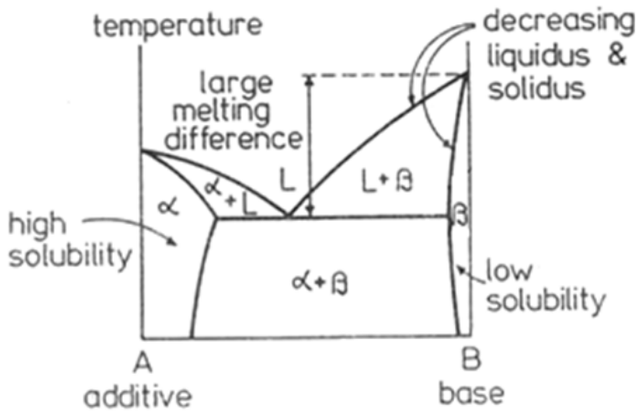

Fig. 12. An ideal phase diagram for the activated sintering system [45].

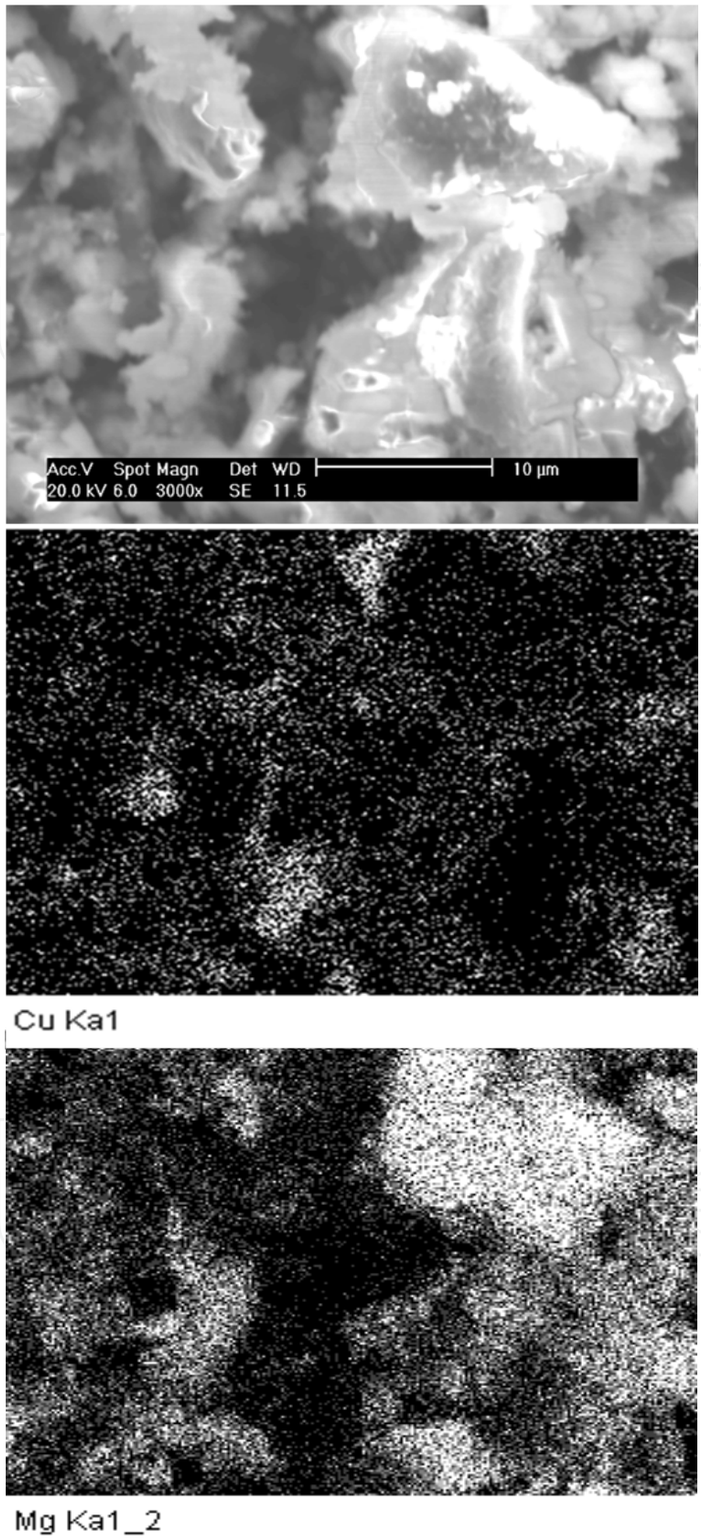

Fig. 13. A secondary electron image and elemental maps of Cu and Mg for $(Mg_{1.1}B_2)_{0.8}Cu_{0.2}$ sample sintered at 575 °C for 5 h [46].

In addition, following these criteria and inspection of the appropriate binary phase diagrams of the additive metal elements with Mg, effective activated addition for the low temperature sintering of MgB_2 could be achieved potentially using lots of candidate metals. Accordingly, Cu was finally determined as effective activator for improving sintering efficiency of MgB_2 in our work.

3. The effect of Cu activator on the microstructure and superconductive properties of MgB_2 prepared by sintering

Cu addition can improve the sintering efficiency of MgB_2 and thus selected as sintering activator. However, whether Cu activator optimizes the microstructure and superconductive properties of MgB_2? To answer this question, the effect of Cu activator on the microstructure of MgB_2 sintered at both low temperature and high temperature were investigated in detail.

3.1 Effect of Cu activator on the reduction of MgO impurity in MgB_2 sintered at high temperature

MgO is always present as the inevitable impurity phase during the sintering process of MgB_2 for the reason that Mg is very reactive with oxygen, which can be supplied by the gaseous O impurity in the protective Ar gas and the oxide impurity (such as B_2O_3 impurity in the B powders) in the starting materials. The presence of MgO impurity may be of great importance and yields a significant effect on the superconductive properties of MgB_2 superconductor. Although the MgO nanoinclusions within MgB_2 grains could serve as strong flux pinning centers when their size were comparable to the coherent length of MgB_2 (.approximately 6~7 nm), the presence of excess MgO phases or largesized MgO particles at the grain boundaries could result in the degradation of grain connectivity [49, 50]. Hence, it is essentially important to control the amount of MgO impurity during the sintering of MgB_2 samples.

In our previous work [51], based on the investigation of the effect of minor Cu addition on the phase formation of MgB_2, it is found that the minor Cu addition (<3 at %) could apparently reduce the amount of MgO impurity in the prepared MgB_2 samples, which provided a new route to govern the oxidation of Mg during the in-situ sintering of MgB_2 samples by altering the amount of Cu addition.

Figure 14 shows the X-ray diffraction patterns of the $(Mg_{1.1}B_2)_{1-x}Cu_x$ (x = 0.0, 0.01, 0.03 and 0.10) samples sintered at 850°C for 30min. It can be seen that all the sintered samples contain MgB_2 as the main phase. In the undoped samples, the MgO peaks are easily recognized, which suggests that some Mg was oxidized during the sintering process and thus MgO was the main impurity in the sintered samples. On the other hand, in the diffracted patterns of the Cu-doped samples, all the MgO phase peaks become weaker and even some peaks identified as MgO phase disappear with the amount of Cu addition increasing. This trend can be observed more clearly from the Fig. 15, which shows the most intense peak (the peak of (200) crystal plane) of MgO in the X-ray diffraction patterns of the sintered $(Mg_{1.1}B_2)_{1-x}Cu_x$ (x = 0.0, 0.01 and 0.03) samples. The results suggest that the minor Cu addition can depress the oxidation of Mg apparently during the in-situ sintering of MgB_2 samples.

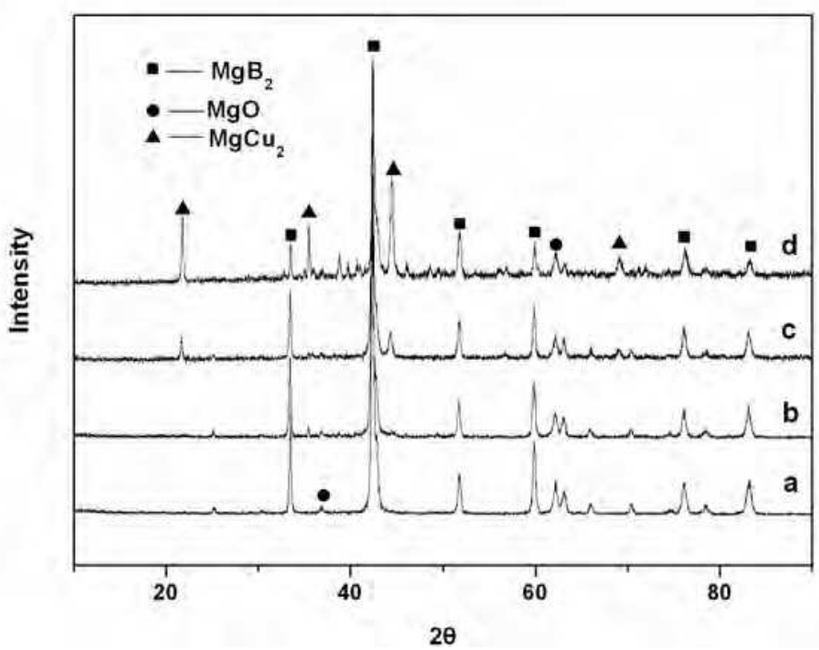

Fig. 14. X-ray diffraction patterns of the prepared $(Mg_{1.1}B_2)_{1-x}Cu_x$ samples sintered at 850°C for 30min with (a) x = 0, (b) x = 0.01, (c) x = 0.03, (d) x=0.10, respectively [51].

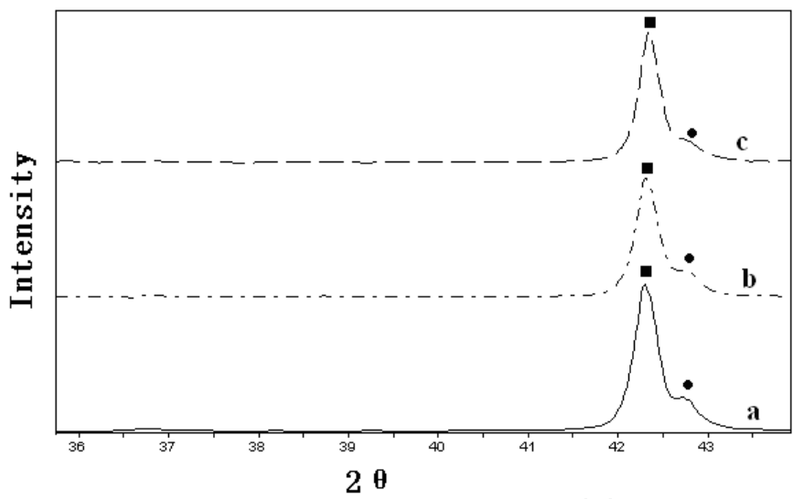

Fig. 15. The enlarged X-ray diffraction patterns around (200) of MgO impurity in the $(Mg_{1.1}B_2)_{1-x}Cu_x$ samples sintered at 850°C for 30min with (a) x = 0, (b) x = 0.01, (c) x = 0.03, respectively [51].

The weight fraction of MgO was calculated from the X-ray diffraction patterns according to the External Standard Method. Fig. 16 shows the weight fraction of MgO versus the amount of Cu addition in the sintered samples. From the figure, it is found that the weight fraction of MgO in the undoped MgB_2 sample is about 16.5%, which is comparable with the previous study [52]. On the other hand, the weight fraction of MgO decreases obviously from 16.5% to 12.5% with the amount of Cu addition increasing from 0.0 to 0.03. However, when the

amount of Cu addition increases from 0.03 to 0.10, the weight fraction of MgO almost remains unchanged (see Fig. 16) while the $MgCu_2$ phase increases significantly (see Fig. 14). The excess Cu addition in the $(Mg_{1.1}B_2)_{0.9}Cu_{0.1}$ sample has no significant effect on the further decrease of MgO impurity. Besides, the excess $MgCu_2$ phase in the $(Mg_{1.1}B_2)_{0.9}Cu_{0.1}$ sample (see Fig. 1) may also depress the superconductivity properties of MgB_2 phase. Hence, we conclude that the x=0.03 Cu addition has the best effect on the decrease of MgO impurity during the in-situ sintering of MgB_2 samples.

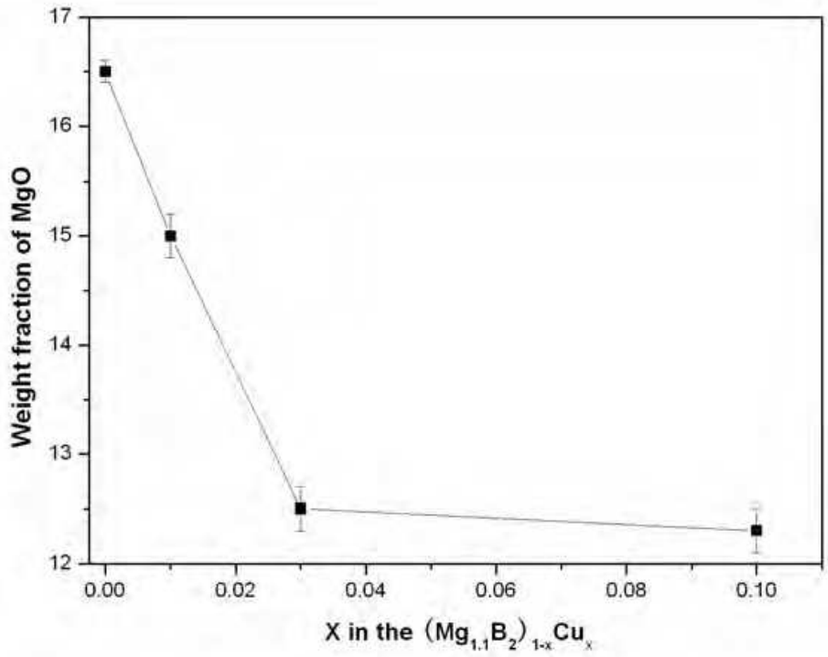

Fig. 16. The weight fraction of MgO versus the amount of Cu addition in the Cu-doped samples sintered at 850 °C for 30 min [51].

The scanning electron microscopy images of the sintered $(Mg_{1.1}B_2)_{1-x}Cu_x$ samples are shown in the Fig. 17. There is an MgO layer on the partial surface of MgB_2 grains in the undoped sample, as shown in Fig. 17a. The MgO layer consists of short MgO whiskers, which is similar with the MgO morphology observed in the study on the oxidation of MgB_2 [53]. On the other hand, in the Cu-doped samples, the amount of MgO impurity decreases with the increasing amount of Cu addition and at the same time the morphology of MgO transits from whiskers to nanoparticles (see Fig. 17b and Fig. 17c). The result of SEM images is consistent with the XRD pattern and they both reveal that the addition of minor Cu can apparently decrease the MgO impurity in the MgB_2 samples. From Fig. 17, it is also found that the MgB_2 grains become larger and more regular accompanying with the increasing amount of Cu addition, which indicates that the Cu addition can also promote the growth of MgB_2 grains at the same time with decreasing the MgO impurity in the prepared MgB_2 samples.

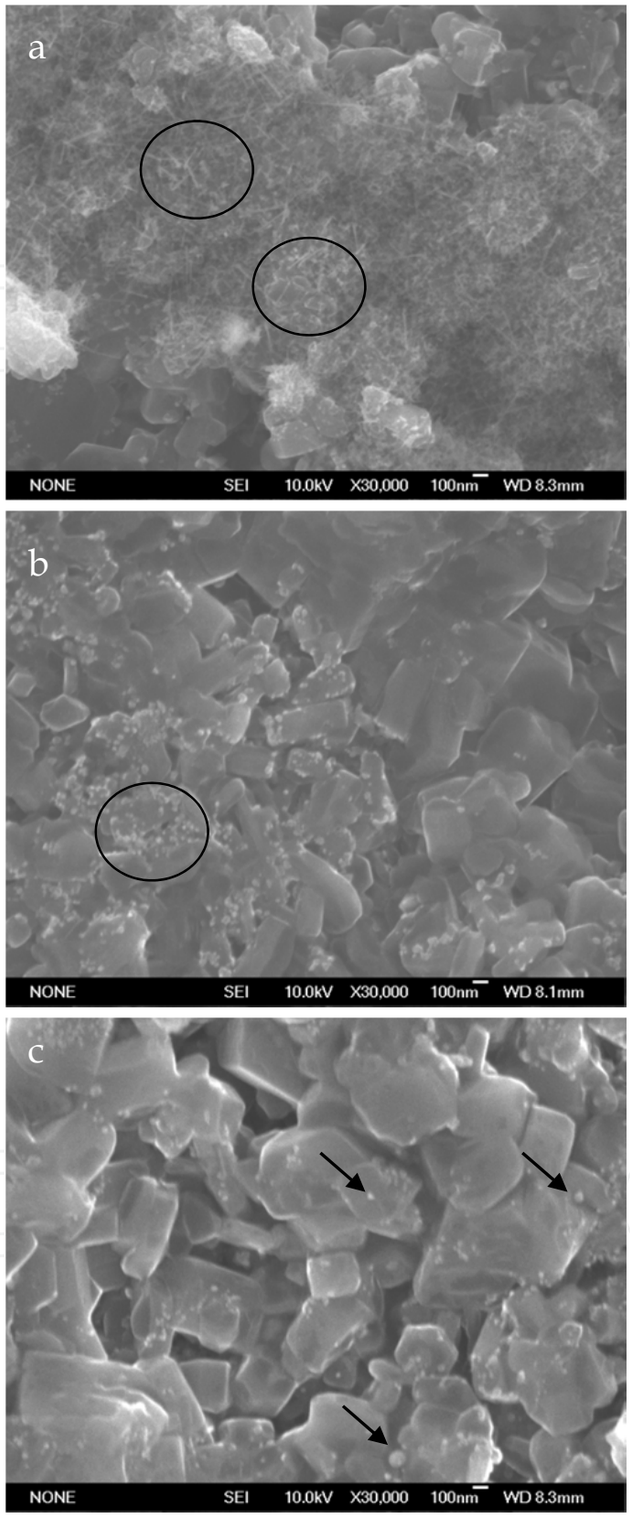

Fig. 17. Scanning electron microscopy images of the $(Mg_{1.1}B_2)_{1-x}Cu_x$ samples sintered at 850 °C for 30 min with (a) x = 0, (b) x = 0.01 and (c) x = 0.03, respectively. The MgO whiskers and nanoparticles are indicated by the black circles and arrows in the figures [51].

In order to investigate the effect of the decreasing MgO impurity induced by the minor Cu addition on the superconductive properties of MgB_2 samples, the corresponding T_c temperatures of all sintered samples were measured. Fig. 18 illustrates the temperature dependence of resistivity for the $(Mg_{1.1}B_2)_{1-x}Cu_x$ (with x = 0, 0.01 and 0.03) samples sintered at 850 °C for 30min. As shown in it, the undoped sample exhibits a slight suppression in the value of T_c compared to the typical pure MgB_2 samples, which can be attributed to the limit of MgB_2 intergranular connection caused by the excessive MgO impurity at the grain boundaries. However, in the Cu-doped samples, the values of T_c are over 38K and slightly increase from 38.1 K to 38.6 K with the increasing amount of Cu addition from x = 0.01 to x = 0.03, which is comparable to the pure MgB_2 samples (39 K). The observation could be explained by the decrease of MgO impurity and the growth of MgB_2 grains resulting from the minor Cu addition.

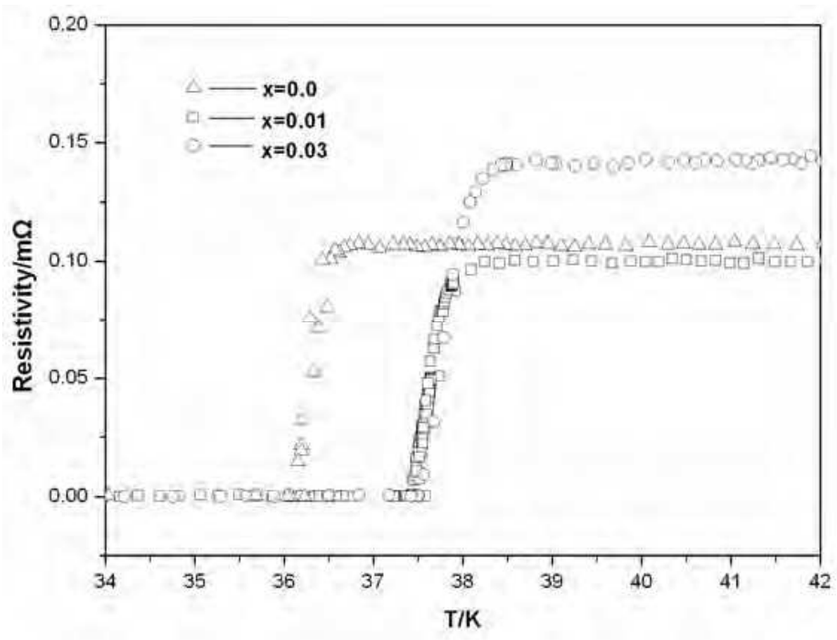

Fig. 18. The temperature dependence of resistivity for the $(Mg_{1.1}B_2)_{1-x}Cu_x$ (x = 0, 0.01 and 0.03) samples sintered at 850 °C for 30min [51].

In summary, the minor Cu addition can decrease the amount of MgO impurity and thus significantly improve the superconductive properties of MgB_2 bulks. However, how the Cu addition avoids the oxidation of Mg during the sintering process of MgB_2 is still to be answered.

It has been indicated that during the sintering process of Mg-Cu-B system, the Mg-Cu liquid locally formed firstly in the presence of Cu through an eutectic reaction. The local Mg-Cu liquid appearing at such low temperature could dissolve some Mg and wrap the neighboring Mg particles, which partly avoided Mg contacting with the gaseous O existing in the interspace of the pressed samples and the oxide impurity (such as B_2O_3 in the B powders) in the starting materials. Hence, the oxidation of Mg during the low-temperature (below the Mg melting point) sintering stage resulting from the gaseous O existing in the

interspace and the oxide impurity in the starting materials can be depressed by the presence of local Mg-Cu liquid significantly.

When the temperature was above the Mg melting point (about 650 °C) during the sintering process, the unreacted Mg after the solid reaction stage would melt and volatilize severely as a result of the high vapor pressure of Mg liquid. The gaseous Mg mixed with the protective Ar gas and could react with the O_2 impurity in the protective Ar gas at such high temperature, which resulted in the increasing amount of MgO impurity deposited in the undoped MgB_2 samples after cooling to room temperature [54], as shown in Fig. 17a. On the other hand, the Cu addition could lower the melting point of Mg at the same time of decreasing the vapor pressure of Mg liquid at high temperature [55]. The decrease of the vapor pressure of Mg liquid led by the Cu addition could reduce the amount of the gaseous Mg from the volatilization of Mg, which thus decrease the amount of MgO impurity resulting from the oxidation of gaseous Mg in the doped samples (as shown in Fig. 17b and 17c).

3.2 The synthesis of lamellar MgB_2 crystalline by Cu activated sintering at low temperature

The microstructure of MgB_2 synthesized by Cu activated sintering at low temperature was also investigated in detail [56]. The SEM images of both sintered Cu-doped sample and undoped sample are illustrated in Fig. 19. Lamellar MgB_2 grains with typical hexagonal shape were observed in the Cu-doped sample sintered at low temperature (see Fig. 19a, denoted by the black arrows). There are few impurities between lamellar MgB_2 grains in the MgB_2 region and the Mg-Cu impurities mainly distribute in the region near the lamellar MgB_2 grains, as shown in Fig. 19a. One can also find that all of the MgB_2 grains in the lamellar structure almost share the same orientation except only a few of them. On the other hand, the MgB_2 grains in the undoped sample sintered at high temperature are nearly in the same size as those in the Cu-doped samples and most of them also exhibit typical hexagonal shape. But their orientation is random, which is the typical characteristic of MgB_2 grains sintered in the traditional solid-state sintering (see Fig. 19b). Hence, the MgB_2 grains in the lamellar structure seem to be in better connectivity with each other and there are also fewer voids between them when compared to the MgB_2 grains in the random orientation, as shown in Fig. 19.

It is proposed that Mg atoms could easily diffuse into B through the path of local Mg-Cu liquid and then react with B forming MgB_2 at the interface between Mg-Cu liquid and B particles. Since the local Mg-Cu liquid only serves as the path for the diffusion of Mg into B and does not react with B until all the Mg is run out, it is always present and provide the constant liquid environment for the nucleation and growth of MgB_2 grains. As we all known, there are two main mechanism forming the lamellar crystalline in the liquid sintering environment, two dimensional nucleation and screw dislocation nucleation. The concentration gradient is the driving force for both mechanisms during the isothermal liquid sintering. The surface of the grains in the lamellar crystalline formed following the two dimensional nucleation are generally more smooth and regular than the screw dislocation [57]. On the other hand, the two dimensional nucleation also needs higher supersaturation than the screw dislocation [58]. In present case, the surface of MgB_2 grains in the lamellar crystalline is smooth and regular and no obvious dislocations and impurities are observed.

Moreover, the supersaturation of MgB_2 in the Mg-Cu liquid must be high enough for the two dimensional nucleation due to the comparable less amount of Mg-Cu liquid (the amount of Cu addition is only 8 at%). Hence, it is proposed that the formation mechanism of the present lamellar MgB_2 grains is attributed to the two dimensional nucleation. The energy barrier of the two dimensional nucleation could be defined as follows:

$$(C / Ce)_{crit} = \exp(\pi h \Omega r^2 / 65k^2T^2) \tag{6}$$

$(C / Ce)_{crit}$ is the critical supersaturation, h is the step height, Ω is the atomic volume, r is the surface energy of crystal, k is the Boltzmann constant and T is the sintering temperature. It can be seen that the energy barrier of the two dimensional nucleation mainly depends

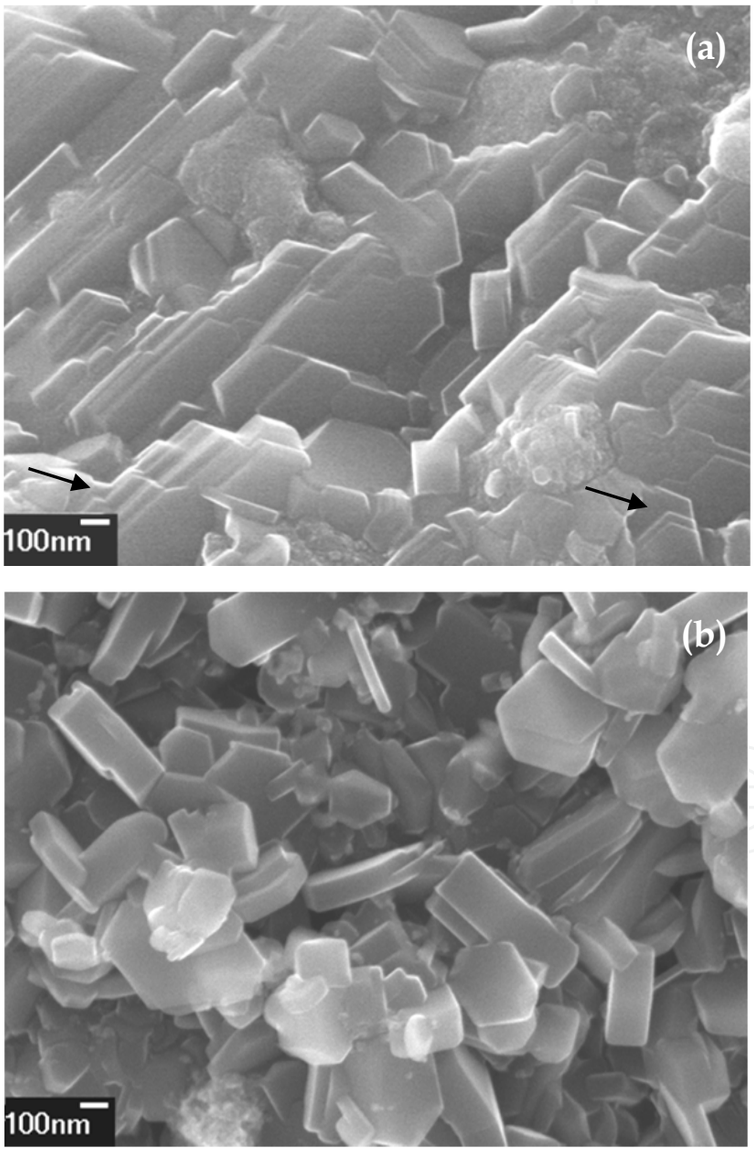

Fig. 19. The SEM images of sintered samples with (a) the Cu-doped sample sintered at 575 °C for 5h and (b) the undoped sample sintered at 750 °C for 1h [56].

on the step height and the surface energy of MgB_2 crystal. On the other hand, only when the MgB_2 supersaturation in the Mg-Cu liquid is higher than the critical supersaturation, the nucleation can start on the surface of B and form the new step. After that, the MgB_2 grains easily grow at this step and form a crystal layer. Accordingly, the schematic of the formation mechanism of the lamellar MgB_2 crytalline is shown in the Fig. 20 with (a) the initial stage, (b) the nucleation and growth stage and (c) the final stage. At the initial stage, the Mg that diffused to the surface of B through the Mg-Cu liquid would react with B as below: Mg + 2B = MgB_2, which can result in the concentration gradient of Mg in the interface (see Fig. 20a). As a result, a lot of Mg could diffuse into the interface and react with B forming MgB_2. Most of produced MgB_2 is dissolved in the Mg-Cu liquid and some MgB_2 will be physically absorbed on the surface of B. When the MgB_2 supersaturation is higher than the critical value for the nucleation, these absorbed MgB_2 will form two dimensional nuclei and produce a new step through the thermodynamic fluctuation. And then the dissolved MgB_2 will deposit on this step and the MgB_2 grains could rapidly grow on this step and form the crystal layer (see Fig. 20b). The new nuclei will continuously forming on the surface of MgB_2 crystal layer and then a new crystal layer will form again. As a result, the lamellar MgB_2 grains are obtained (see Fig. 20c).

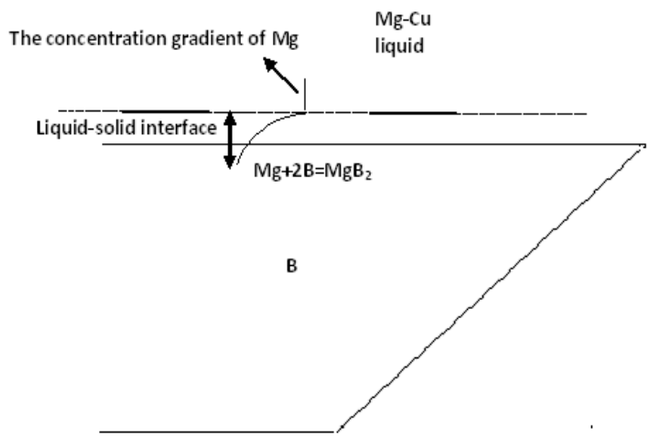

(a)

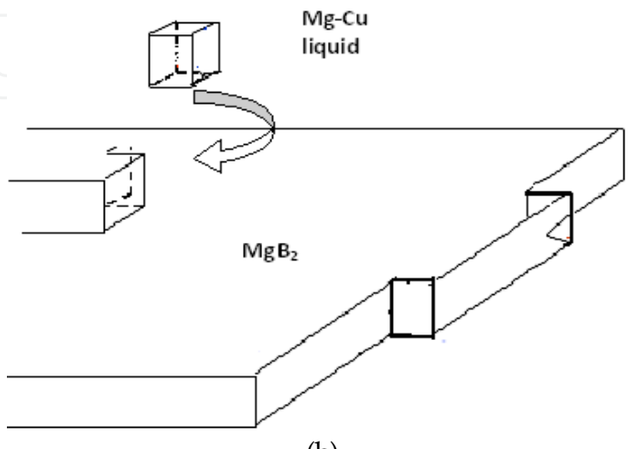

(b)

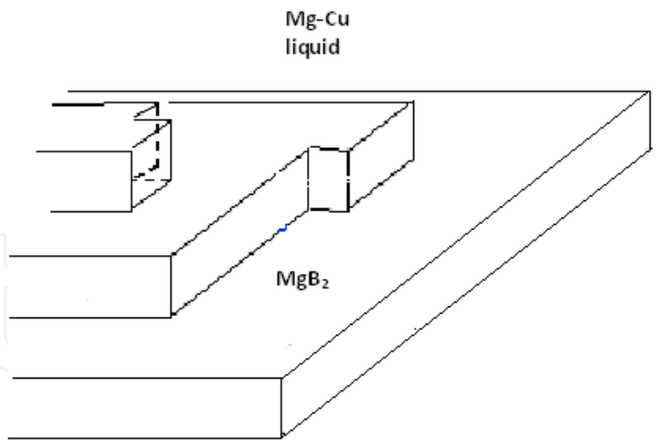

(c)

Fig. 20. The schematic of the formation mechanism of the lamellar MgB_2 crytalline with (a) the initial stage, (b) the nucleation and growth stage and (c) the final stage [56].

Fig. 21 shows the temperature dependence of resistivity of the Cu-doped sample and undoped sample. The resistivity of the Cu-doped samples is much lower than the undoped sample in the measured temperature region from 300K to 40K. The resistivity of MgB_2 sample should be increased with the addition of Cu, as reported previously [59]. Since the Mg-Cu alloys mainly concentrate around the voids and do not degrade the grain connectivity of MgB_2 phase in present sample, the resistivity is ought to keep unchanged and should not be lower than the undoped sample. Hence, the abnormal low resistivity must be attributed to the lamellar structure of MgB_2 grains.

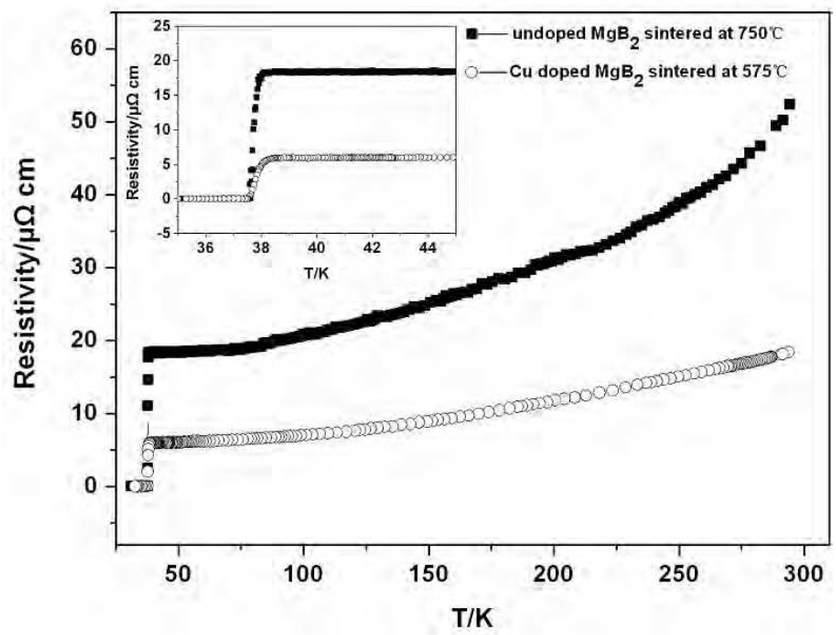

Fig. 21. The temperature dependence of resistivity of the Cu-doped sample and undoped sample [56].

According to the Rowell connectivity analysis, the calculated active cross-sectional area fraction (A_F) represents the connectivity factor between adjacent grains [60]. Here the A_F is estimated as:

$$A_F = \Delta \rho_{ideal} / (\rho_{300K} - \rho_{40K}) \quad (7)$$

$$\Delta \rho_{ideal} = \rho_{ideal(300K)} - \rho_{ideal(40K)} \quad (8)$$

Where ρ_{ideal} is the resistivity of a reference crystal and ρ_T is our measured resistivity at temperature T.

According to the previous studies [13, 60, 61], here the $\Delta \rho_{ideal}$ is 7.3 μΩcm. The results are listed in the Table 3. The value of A_F in the present undoped sample is comparable to that of samples sintered under the similar condition in previous reports [60]. The Cu-doped sample exhibits very excellent A_F, more than two times higher than that of the undoped samples. To further analyze the intergrain connectivity, the residual resistivity ratio (RRR) defined by ρ_{300K} / ρ_{40K} was also estimated, as shown in Table 3. All of the above results indicate that the lamellar MgB_2 grains possess much better grain connectivity than the typical morphology of MgB_2 grains. It should be pointed out that the onset of the transition temperature ($T_{c(onset)}$) of the Cu-doped sample is higher than that of undoped samples, which might be due to better connectivity and higher crystallinity of the lamellar grains (see Fig. 20a and Fig. 20b). However, the width of transition (ΔT_c) of the Cu-doped sample becomes a little wider than that of undoped sample. The transition broadening can be caused by the small grain size, inhomogeneity, impurities and so on. In present case, the lamellar MgB_2 grains shared the same orientation and lead to the intrinsic inhomogeneity in the doped sample, which could be the main factor broadening the transition width.

samples	ΔT_c (K)	$T_{c(onset)}$ (K)	ρ_{40K} (μΩcm)	ρ_{300K} (μΩcm)	RRR	A_P
Undoped MgB_2	0.25	38.0	18.388	51.449	2.780	0.221
Cu-doped MgB_2	0.40	38.3	5.980	18.355	3.069	0.590

Table 3 The transition temperature ($T_{c(onset)}$), width of transition (ΔT_c), measured resistivity values, residual resistivity ratio (RRR) and active cross-sectional area fraction (A_F) for Cu-doped sample and undoped sample, respectively.

In summary, the lamellar MgB_2 grains can be obtained by Cu-activated sintering at low temperature. This lamellar MgB_2 grains possess much better grain connectivity than the typical morphology of MgB_2 grains synthesized by the traditional solid-state sintering. Together with the proper methods increasing the pinning, the present lamellar MgB_2 grains might result in the further improvement of J_c.

4. References

[1] J. Nagamatsu, N. Nakagawa, T. Muranaka, Y. Zentani and J. Akimitsu: Nature, 2001 410 63-64.

[2] D.C. Larbalestier, L.D. Cooley, M.O. Rikel, A.A. Polyanskii, J. Jiang, S. Patnaik, X.Y. Cai, D.M. Feldmann, A. Gurevich, A.A. Squitieri, M.T. Naus, C.B. Eom, E.E. Hellstrom,

R.J. Cava, K.A. Regan, N. Rogado, M.A. Hayward, T. He, J.S. Slusky, P. Khalifah, K. Inumaru and M. Haas: Nature, 2001 410 186-189.
[3] K. Kawano, J.S. Abell, M. Kambara, N. Hari Babu and D.A. Cardwell: Appl. Phys. Lett., 2001 79 2216.
[4] V. Cambel, J. Fedor, D. Gregusova, P. Kovac and I. Husek: Supercond. Sci. Technol., 2005 18 417.
[5] V. Braccini, D. Nardelli, R. Penco and G. Grasso: Physica C, 2007 456 209-217.
[6] A. Serquis, L. Civale, J.Y. Coulter, D.L. Hammon, X.Z. Liao, Y.T. Zhu, D.E. Peterson, F.M. Mueller, V.F. Nesterenko and S.S. Indrakanti: Supercond. Sci. Technol., 2004 17 L35-L37.
[7] D. Mijatovic, A. Brinkman, D. Veldhuis, H. Hilgenkamp, H. Rogalla, G. Rijnders, D.H.A. Blank, A. V. Pogrebnyakov, J.M. Redwing, S.Y. Xu, Q. Li and X.X. Xi: Appl. Phys. Lett, 2005 87 192505.
[8] S.A. Cybart, K. Chen, Y. Cui, Q. Li, X.X. Xi and R.C. Dynes: Appl. Phys. Lett., 2006 88 012509.
[9] K. Chen, Y. Cui, Q. Li, X.X. Xi, S.A. Cybart, R.C. Dynes, X. Weng, E.C. Dickey and J.M. Redwing: Appl. Phys. Lett., 2006 88 222511.
[10] S. Jin, H. Mavoori, C. Bower and R.B. van Dover: Nature, 2001 411 563-565.
[11] S. Jin, R.C. Sherwood, R.B. Vandover, T.H. Tiefel and D.W. Johnson: Appl. Phys. Lett., 1987 51 203-204.
[12] H. Kumakura, A. Matsumoto, H. Fujii and K. Togano: Appl. Phys. Lett., 2001 79 2435-2437.
[13] P.C. Canfield, D.K. Finnemore, S.L. Bud'ko, J.E. Ostenson, G. Lapertot, C.E. Cunningham and C. Petrovic: Phys. Rev. Lett., 2001 86 2423-2426.
[14] A. Serquis, L. Civale, D.L. Hammon, J.Y. Coulter, X.Z. Liao, Y.T. Zhu, D.E. Peterson and F.M. Mueller: Appl. Phys. Lett., 2003 82 1754-1756.
[15] P.C. Canfield, D.K. Finnemore, S.L. Bud'ko, J.E. Ostenson, G. Lapertot, C.E. Cunningham and C. Petrovic: Phys. Rev. Lett., 2001 86 2423-2426.
[16] A.N. Baranov, V.L. Solozhenko, C. Lathe, V.Z. Turkevich and Y.W. Park: Supercond. Sci. Technol., 2003 16 1147-1151.
[17] J.C. Grivel, R. Pinholt, N.H. Andersen, P. Kovac, I. Husek and J. Homeyer: Supercond. Sci. Technol., 2006 19 96-101.
[18] Q.R. Feng, X. Wang, X.Y.Wang and G.C. Xiong: Solid State Commun., 2002 122 459.
[19] Q.R. Feng, X. Chen, Y.H. Wang, X. Wang, G.C. Xiong and Z.X. Gao: Physica C, 2003 386 653.
[20] Q.R. Feng, C. Chen, J. Xu, L.W. Kong, X. Chen, Y.Z. Wang, Y. Zhang and Z.X. Gao: Physica C, 2003 411 41-46.
[21] W. Goldacker, S.I. Schlachter, B. Obst and M. Eisterer: Supercond. Sci. Technol., 2004 17 S490.
[22] M. Bhatia, M.D. Sumption, S. Bohnenstiehl, S.A. Dregia, E.W. Collings, M. Tomsic and M. Rindfleisch: IEEE Trans Appl. Suprcond., 2007 17 2750-2753.
[23] G.H.S. Price: Int. Met., 1938 62 143.
[24] W.Z. Ostwald: Phys. Chem., 1900 34 495.
[25] W. Goldacker, S.I. Schlachter, B. Obst, B. Liu, J. Reiner and S. Zimmer: Supercond. Sci. Technol., 2004 17 S363–S368.
[26] M. Maeda, Y. Zhao, S.X. Dou, Y. Nakayama, T. Kawakami, H. Kobayashi and Y. Kubota: Supercond. Sci. Technol., 2008 21 032004.
[27] S. Soltanian, X.L. Wang, J. Horvat, S.X. Dou, M.D. Sumption, M. Bhatia, E.W. Collings, P. Munroe and M. Tomsic: Supercond. Sci. Technol., 2005 18 658–666.

[28] W.K. Yeoh, J. Horvat, J.H. Kim, X. Xu and S.X. Dou: Appl. Phys. Lett., 2007 90 122502.
[29] Y.C. Liu, Q.Z. Shi, Q. Zhao and Z.Q. Ma: J. Mater. Sci: Mater. Electron., 2007 18 855.
[30] M.S.A. Hossain, J.H. Kim, X. Xu, X.L. Wang, M. Rindfleisch, M. Tomic, M.D. Sumption, E. WCollings and S.X. Dou: Supercond. Sci. Technol., 2007 20 L51–L54.
[31] J.H. Kim, X. Xu, M.S.A. Hossain, D.Q. Shi, Y. Zhao, X.L. Wang, S.X. Dou, S. Choi and T. Kiyoshi: Appl. Phys. Lett., 2008 92 042506.
[32] G.H.S. Price: Int. Met., 1938 62 143.
[33] W.Z. Ostwald: Phys. Chem., 1900 34 495.
[34] N. Rogado, M.A. Hayward, K.A. Regan, Y. Wang, N.P. Ong, H.W. Zandbergen, J.M. Rowell and R.J. Cava: J. Appl. Phys., 2002 91 274-277.
[35] A.Yamamoto, J. Shimoyama, S. Ueda, Y. Katsura, S. Horii and K. Kishio: Supercond. Sci. Technol., 2005 18 116-121.
[36] W. Goldacker, S.I. Schlachter, B. Obst, B. Liu, J. Reiner and S. Zimmer: Supercond. Sci. Technol. 2004 17 S363–S368.
[37] M. Maeda, Y. Zhao, S.X. Dou, Y. Nakayama, T. Kawakami, H. Kobayashi and Y. Kubota: Supercond. Sci. Technol., 2008 21 032004.
[38] Z.Q. Ma and Y.C. Liu: Mater. Chem. Phys., 2011 126 114-117.
[39] Q.Z. Shi, Y.C. Liu, Q. Zhao and Z.Q. Ma: J. Alloys Compd., 2008 458 553-557.
[40] J. Shimoyama, K. Hanafusa, A. Yamamoto, Y. Katsura, S. Horii, K. Kishio and H. Kumakura: Supercond. Sci. Technol., 2007 20 307-311.
[41] Y. Hishinuma, A. Kikuchi, Y. Iijima, Y. Yoshida, T. Takeuchi and A. Nishimura: IEEE Trans. Appl. Supercond., 2007 17 2798-2801.
[42] Z.Q. Ma, Y.C. Liu, Q.Z. Shi, Q. Zhao and Z.M. Gao: Supercond. Sci. Technol., 2008 21 065004.
[43] Z. Q. Ma, H. Jiang and Y. C. Liu: Supercond. Sci. Technol., 2010 23 025005.
[44] J.C. Grivel, A. Abrahamsen and J. Bednarcik: Supercond. Sci. Technol., 2008 21 035006.
[45] C.M. Kipphut and R.M. German: Sci. sintering, 1988 20 31-41.
[46] Z.Q. Ma, Y.C. Liu, Q.Z. Shi, Q. Zhao and Z.M. Gao: Mater. Res. Bull., 2009 44 531-537.
[47] D.K. Finnemore, J.E. Ostenson, S.L. Bud'ko, G. Lapertot and P.C. Canfield: Phys. Rev. Lett., 2001 86 2420-2422.
[48] The Materials Information Society, Binary Alloy Phase Diagram, 2nd edn plus updates, Metals Park, OH: ASM International (1996).
[49] J.H. Kim, S.X. Dou, D.Q. Shi, et al: Supercond. Sci. Technol., 2007 20 1026-1031.
[50] C.H. Jiang, H. Hatakeyama, H. Kumakura: Physica C, 2005 423 45-50.
[51] Z. Q. Ma, Y.C. Liu, Q.Z. Shi, Q. Zhao and Z.M. Gao: J. Alloys Compd. 2009 471 105-108
[52] J.H. Kim, S.X. Dou, J.L. Wang, et al: Supercond. Sci. Technol., 2007 20 448-451.
[53] D. Yang, H. Sun, H. Lu, et al: Supercond. Sci. Technol., 2003, 16 576-581
[54] X.Z. Liao, A.C. Serquis, Y.T. Zhu, et al: Appl. Phys. Lett., 2002 80 4398-4400.
[55] V. Ganesan, H. Feufel, F. Sommer, et al: Metall. Mater. Trans. B, 1998 29 807-813.
[56] Z. Q. Ma, Y.C. Liu and Z.M. Gao: Scripta Mater. 2010 63 399-402
[57] A. E. Nielsen: *J. Crystal Growth,* 1984 67 289-310.
[58] L. M. Fabietti and R. Trivedi: *Metall. Trans. A,* 1991 22 1249-1258
[59] K. Singh, R. Mohan, N. Kaur, N. K. Gaur, M. Dixit, V. Shelke and R. K. Singh: *Physica C*, 2006 450 124–128.
[60] J. M. Rowell, S. Y. Xu, X. H. Zeng, A. V. Pogrebnyakov, Q. Li, X. X. Xi, J. M. Redwing, W. Tian and X. Pan: *Appl Phys Lett*, 2003 83 102-104.
[61] R. H. T. Wilke, S. L. Bud'ko, P. C. Canfield, D. K. Finnemore, R. J. Suplinskas and S. T. Hannahs: *Physica C,* 2005 424 1-16.

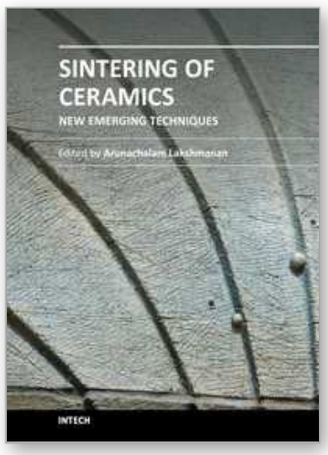

Sintering of Ceramics - New Emerging Techniques

Edited by Dr. Arunachalam Lakshmanan

ISBN 978-953-51-0017-1
Hard cover, 610 pages
Publisher InTech
Published online 02, March, 2012
Published in print edition March, 2012

The chapters covered in this book include emerging new techniques on sintering. Major experts in this field contributed to this book and presented their research. Topics covered in this publication include Spark plasma sintering, Magnetic Pulsed compaction, Low Temperature Co-fired Ceramic technology for the preparation of 3-dimesinal circuits, Microwave sintering of thermistor ceramics, Synthesis of Bio-compatible ceramics, Sintering of Rare Earth Doped Bismuth Titanate Ceramics prepared by Soft Combustion, nanostructured ceramics, alternative solid-state reaction routes yielding densified bulk ceramics and nanopowders, Sintering of intermetallic superconductors such as MgB2, impurity doping in luminescence phosphors synthesized using soft techniques, etc. Other advanced sintering techniques such as radiation thermal sintering for the manufacture of thin film solid oxide fuel cells are also described.

INTECH
open science | open minds

InTech Europe
University Campus STeP Ri
Slavka Krautzeka 83/A
51000 Rijeka, Croatia
Phone: +385 (51) 770 447
Fax: +385 (51) 686 166
www.intechopen.com

InTech China
Unit 405, Office Block, Hotel Equatorial Shanghai
No.65, Yan An Road (West), Shanghai, 200040, China
中国上海市延安西路65号上海国际贵都大饭店办公楼405单元
Phone: +86-21-62489820
Fax: +86-21-62489821

IntechOpen